17th World Conference on Earthquake Engineering, 17WCEE
Sendai, Japan - September 13th to 18th 2020

TESTS OF SCALED PILE CAPS, PART 2: EFFECT OF REINFORCEMENT STRAIN ON COMPRESSIVE FAILURE

T. Ichinose[(1)], L. Laughery[(2)], K-Y. Liu[(3)], S. Komatsu[(4)],
K-Y. Liu[(5)], Y. Nakagami[(6)], T. Matsunoshita[(7)], K. Kasai[(8)]

[(1)] *Professor, Nagoya Institute of Technology, ich@nitech.ac.jp*
[(2)] *Associate, Exponent, llaughery@exponent.com*
[(3)] *Associate Professor, National Cheng Kung University, kyliu@gs.ncku.edu.tw*
[(4)] *Assistant Professor, Shimane University, s.komatsu@riko.shimane-u.ac.jp*
[(5)] *Graduate Student, National Cheng Kung University, ckck89105@gmail.com*
[(6)] *Graduate Student, Nagoya Institute of Technology, yohhen031@gmail.com*
[(7)] *Undergraduate Student, Nagoya Institute of Technology, nnknlturjn@gmail.com*
[(8)] *Professor, Tokyo Institute of Technology, kasai.k.ac@m.titech.ac.jp*

Abstract

Twelve triangular pile caps were tested under uniaxial load until failure. The pile caps were scaled versions of one another, with effective depths of 250mm, 500mm, or 1000mm, shear span ratios of one, and either one or three layers of bottom reinforcement. This paper is the second in a two-part series discussing the test results. Part one presents a summary of the experiment results, and discussion of pile caps failing at small bottom reinforcement strains. This part discusses the effect of the area of bottom reinforcement on strength. In all the specimens, the strain of the reinforcement did not reach the yield strain. The observed strains in the bottom reinforcement agreed with the predictions of the strut-and-tie model irrespective of the reinforcement ratio. The strengths of the specimens with three-layers reinforcement were 1.4 times those with one-layer reinforcement. Noting that $3^{1/3} = 1.4$, we may conclude that the strength of the pile caps was proportional to the reinforcement ratio to the power of 1/3 as assumed in the equation for the shear strength of RC beam of ACI 318-19. However, this result is not consistent with the conclusion of the strut-and-tie model if we assume the strength of each strut to be independent of the strain of the reinforcement. If one assumes linearly-distributed strains with inclined neutral axes located at the lower borders of the struts, one gets strengths of the specimens similar to the observations, as the depths of the struts increased with the amount of bottom reinforcement.

Keywords: Pile cap, Reinforcement, Strut-and-tie model; Strain; Neutral axis

1. Introduction

This paper is the second of a two-part series discussing the experimental program and results. Part one presents the experimental program and results for triangular footings with three layers of bottom reinforcement. The footings were constructed at three scales (S: a=d=250mm, M: a=d=500mm, and L: a=d=1000mm) and with two different bottom reinforcement configurations (1 layer or 3 layers). This paper discusses the effect of the amount of reinforcement on the strength of pile cap. The test results are compared with the strut-and-tie model and a model considering the strain.

2. Equilibrium of strut-and-tie model and steel strain

Figure 1 shows the equilibrium between the vertical load, P, the reaction, Q, the compressive forces of concrete, C, and the tensile forces of reinforcement, T. The equilibrium leads to the following equation for the tensile force and the vertical load.

$$P = 6T\cos 30 \qquad \text{or} \qquad T = \frac{P}{6\cos 30} \tag{1}$$

The inclined orange line in Fig. 2 shows the strain of the bottom reinforcement predicted by Eq. 1 for specimen L1 with one layer of reinforcement. The other lines in Fig. 2 show the observed strains at the locations in Fig. 3. The observed strains agree with the prediction beyond approximately 1000 με. The strains of the other specimens also agreed with the prediction.

Because the reinforcement did not yield in any specimens, the model shown in Fig. 1 also leads to the following equation for the strength of the specimens.

$$P_u = 3Af_c \sin 45 \tag{2}$$

where A is the area of each strut and f_c is the strength of concrete. However, Eq. 2 does not agree with the observation reported in Part 1 paper in two aspects.

(1) Equation 2 does not depend on the amount of the reinforcement. Nevertheless, specimens with three layers of reinforcement were observed to be 1.4 times stronger than those with one layer of reinforcement. Noting that $3^{1/3} = 1.4$, one may conclude that f_c above is not the actual concrete strength but is an *effective* strength which is proportional to the third root of the amount of the reinforcement. In ACI code [1], it is assumed that the shear strength of RC beam is proportional to the reinforcement ratio to the power of 1/3.

(2) P_u in Equation 2 is proportional to the concrete strength. However, the strength of specimen L3H was 1.4 times that of specimen L3a, whereas the concrete compressive strength of specimen L3H was 1.9 times that of specimen L3a. Noting $1.9^{1/2} = 1.4$, one may again conclude that f_c is not the real concrete strength but is an *effective* strength which is proportional to the square root of the actual concrete strength.

In the following sections, we will introduce a new method where we do not need the notion of “effective strength”.

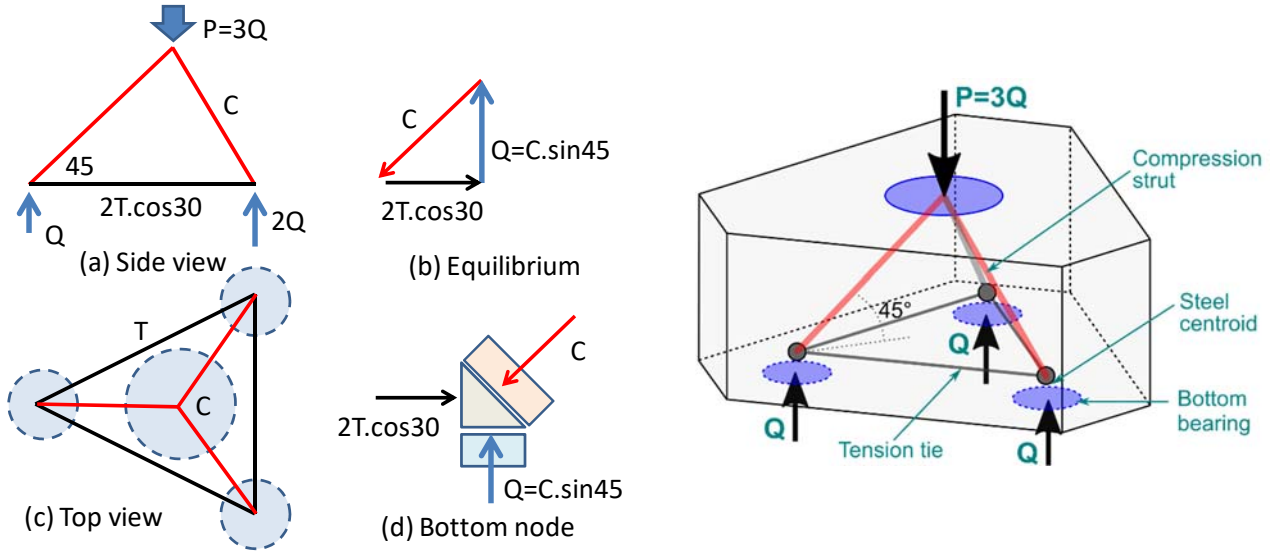

Fig. 1 – Strut-and-tie model

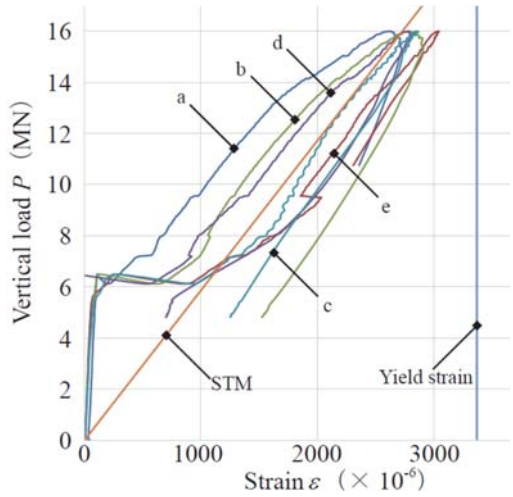

Fig. 2 – Strain vs. vertical load of specimen L1.

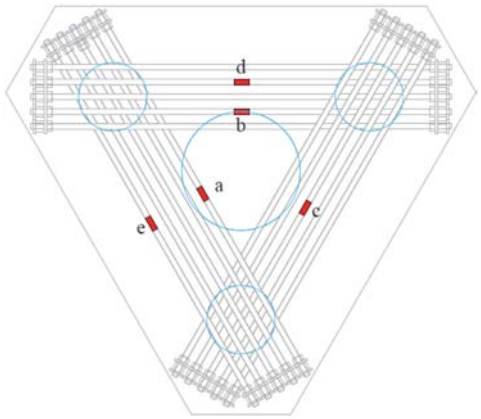

Fig. 3 – Locations of strain gages (specimen L1).

3. Observed Cracks

Figures 4 and 5 show the cracks in specimen L3H at the peak load and after testing, respectively. Fig. 6 and Fig. 7 show the cracks in specimen L1 at the same stages. The flexural cracks indicated by 1 in Fig. 4 occurred first. Second, the inclined cracks indicated by 2 in Fig. 4 occurred. After the peak load, the horizontal cracks indicated by 3 in Fig. 5 were prominent as shown in the photograph in Fig. 8. The cracks of specimen L1 were similar to those of specimen L3H, except that the flexural cracks were more prominent. Fig. 9 shows specimen L1 after the test. The pink circle shows the location of the top loading plate. The inclined surface of the concrete appeared as a result of the spalling of the concrete connecting the top loading plate and the anchor plates of the bottom reinforcement. The implication of Fig. 9 will be discussed later. Fig. 10 shows the sinking of the top plate. Similar sinking was observed in all specimens.

One S3-type specimen was cut after core sampling as shown in Fig. 11. Fig. 12 shows the resulting cross section. Sliding of concrete was observed between the top and bottom plates as shown by the red arrows in this figure.

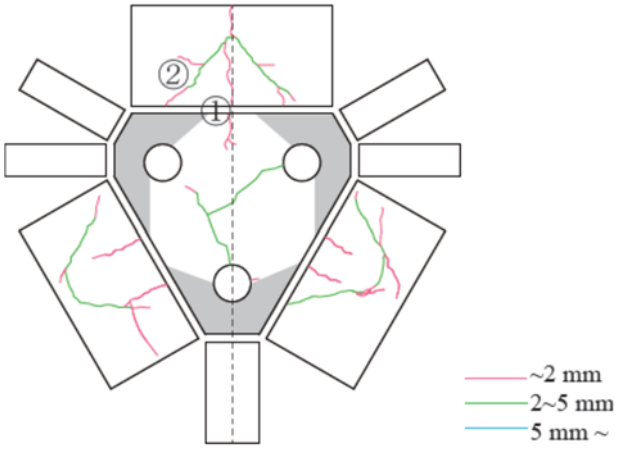

Fig. 4 – Cracks of L3H at peak load.

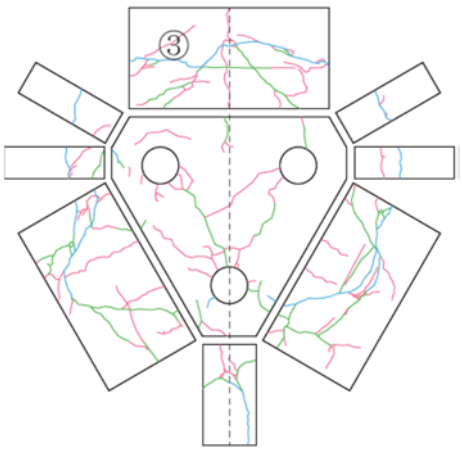

Fig. 5 – Cracks of L3H after test.

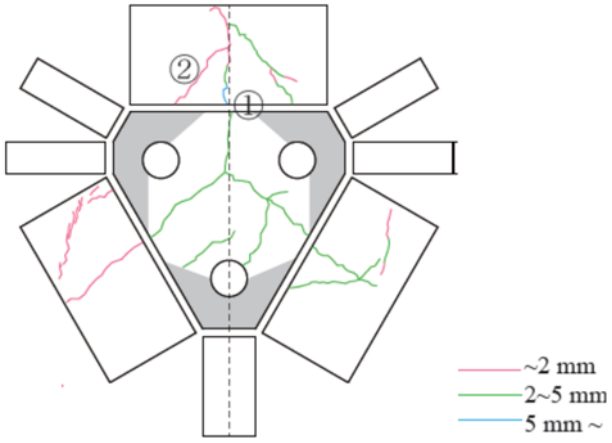

Fig. 6 – Cracks of L1 at peak load.

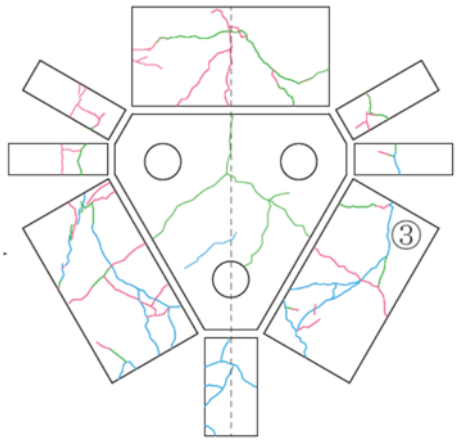

Fig. 7 – Cracks of L1 after test.

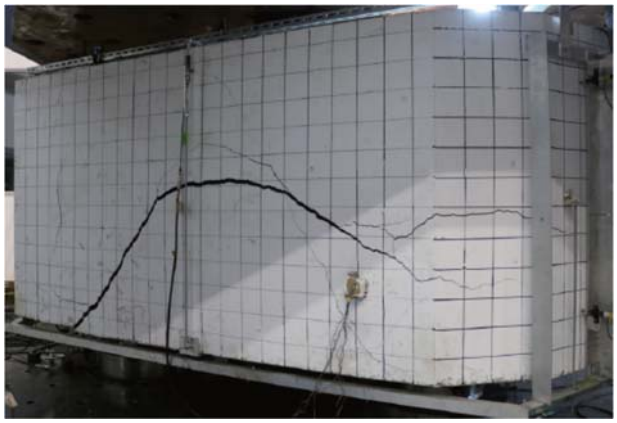

Fig. 8 – Specimen L3H after test.

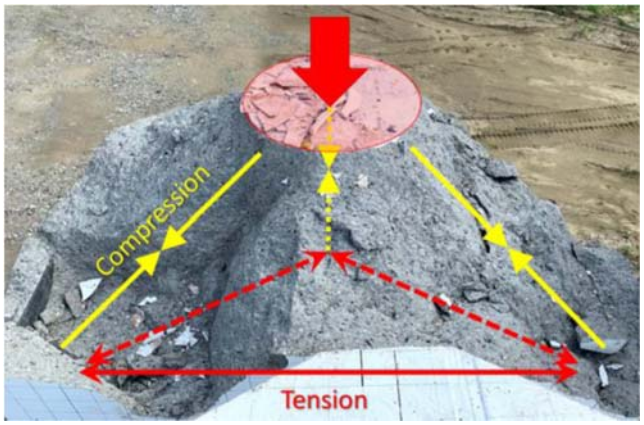

Fig. 9 – Specimen L1 after test indicating the struts.

Fig. 10 – Sinking of top plate of specimen L3a.

Fig. 11 – Cutting specimen S3.

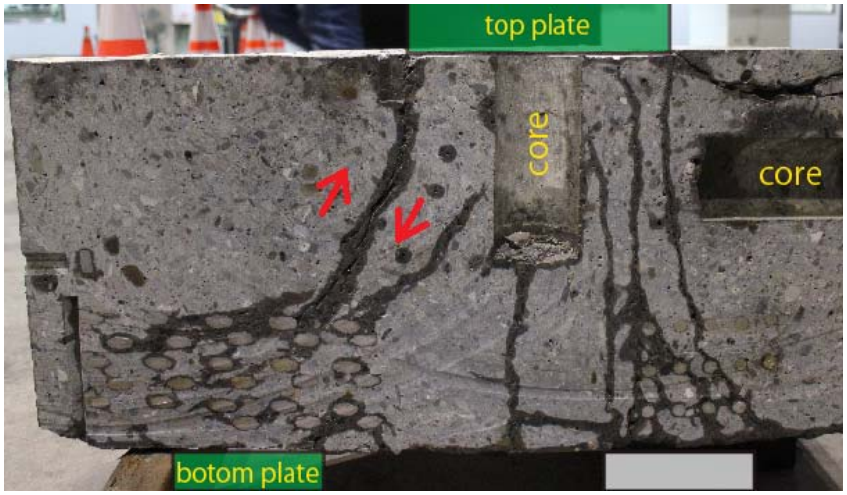

Fig. 12 – Section of specimen S3 (courtesy of Dr. Srinivas Mogili).

4. Deformation of Specimens Inferred from Surface Measurements

The measurement frame for L-type specimens is shown in blue in Fig. 13. The frame was supported by the bolts embedded in the narrower side surfaces of the specimen. The numbers in Fig. 13 show the locations of displacement meters. Meters 1~4 were attached from the measurement frame to the bottom face of the specimen as indicated in Table 1 and Fig. 13d to measure the deflection of the bottom surface relative to the sides. Meters 15~20 were attached from the measurement frame to the side faces of the specimen (Fig. 13a and b) to measure the rotation of the side surfaces. Meters 12~14 (Fig. 13a and b) were connected to bolts embedded in the top and bottom surfaces of the specimens to measure vertical widening caused by the cracks shown in Fig. 8. Meters 7, 8, 11 (Fig. 13c) were attached from the top plate to the adjacent surface of the concrete top to measure sinking of the top plate as shown in Fig. 11. Meters 21~26 (Fig. 13d) were attached from the bottom plate to measure the sinking of the bottom plate.

Table 1 – Locations of displacement meters.

No.	From	To
1 ~ 4	Frame	Concrete bottom
5, 9, 10	BATS platen	Concrete bottom
6	BATS platen	Bottom plate side
7, 8, 11	Top plate	Concrete top
12 ~ 14	Concrete top	Concrete bottom
15 ~ 20	Frame	Concrete side
21 ~ 26	Bottom plate	Concrete bottom
27 ~ 28	Frame	Concrete top

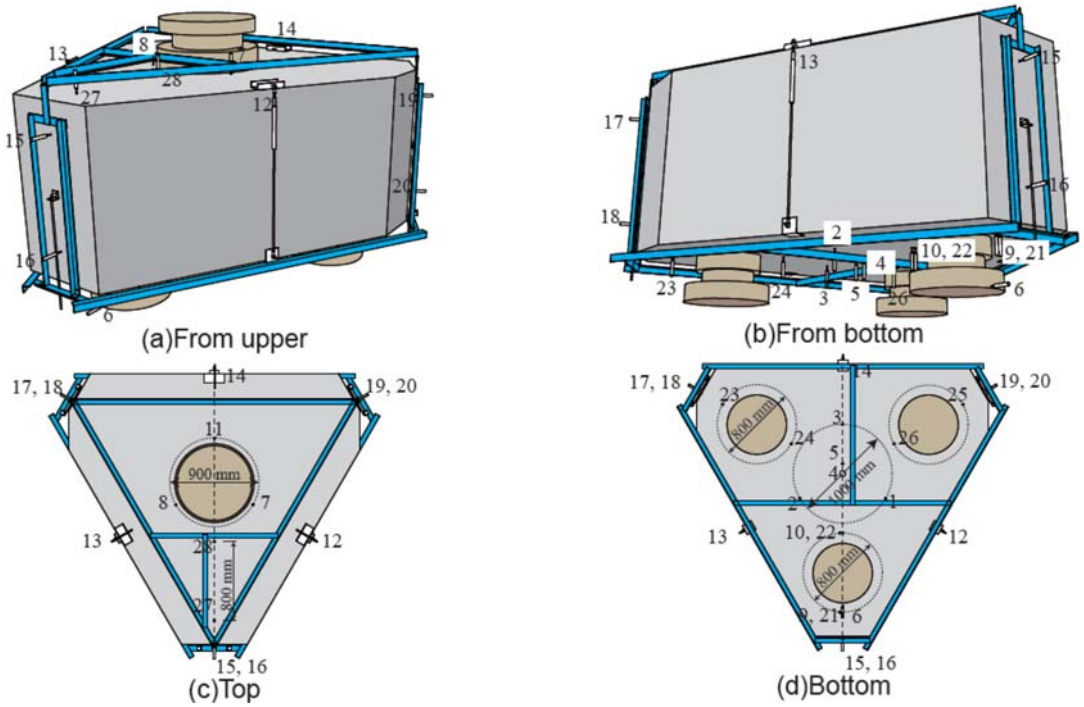

Fig. 13 – Locations of displacement meters for L-size specimens.

Fig. 14 shows the deformation of specimen L3H at the section indicated in Fig. 12 inferred from the displacement transducers shown in Fig. 13 at the deflection of the peak load, δ_p = 5.4 mm. The numbers in parentheses indicate the horizontal and vertical displacement relative to the measurement frame shown in Fig. 13. Detail of the derivation of the displacements from the displacement sensors illustrated in Fig. 13 are described in Ref. [2]. The width of the flexural crack, 2.8 mm, indicates the total of the widths of all flexural cracks. For L3H, sinking of the top plate (3.5 mm) was 65 % of the total deflection (3.5/5.4 = 0.65).

Fig. 15a shows the inferred deformation of L1 at δ_p = 7.3 mm, where the sinking of the top plate increased to 2.8 mm, which is 38 % of the total deflection (2.8/7.3 = 0.38), a much smaller portion than L3H. The sinking of the bottom plate was less than that of the top plate in both specimens. The red arrows in Fig. 14 and Fig. 15a indicate sliding of concrete caused by the inclined compressive stresses shown in Fig. 1.

It should be noted, however, that the volcano-shaped failure shown in Fig. 9 may lead to another interpretation of deformation as shown in Fig. 15b. Here, it is assumed that compressive strain was prominent up to the peak load and the sliding observed in Fig. 12 occurred after the peak. In the case of specimens L3H and L1, the measured sinking of the top plates at the peak deformation were 24 mm and 8 mm, respectively, which were much larger than those at the peak load. If the inclined cracks extending from the upper plate as shown in Fig.

15b are assumed to constitute the surface of a cone as indicated by the red lines in Fig. 16a and b, we obtain a curved crack as shown in Fig. 16c, which looks similar to Fig. 8.

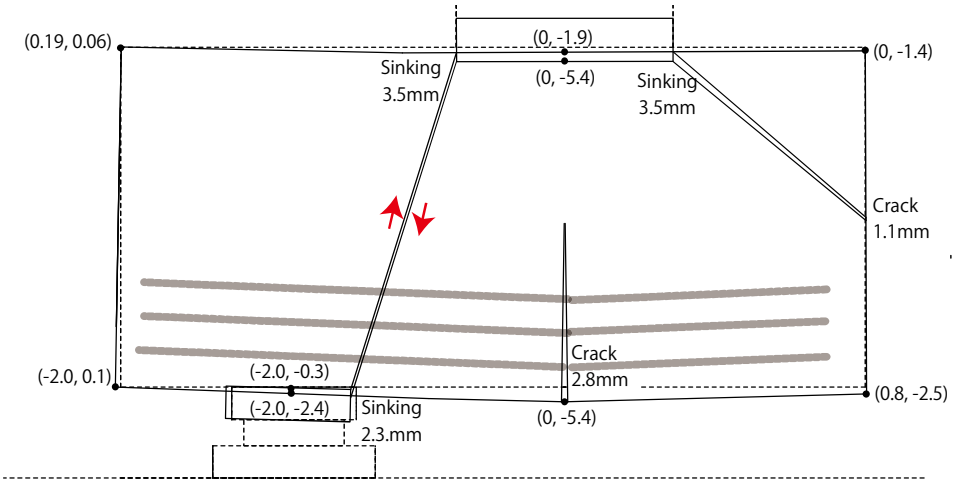

Fig. 14 – Deformation of specimen L3H at the peak load assuming sliding

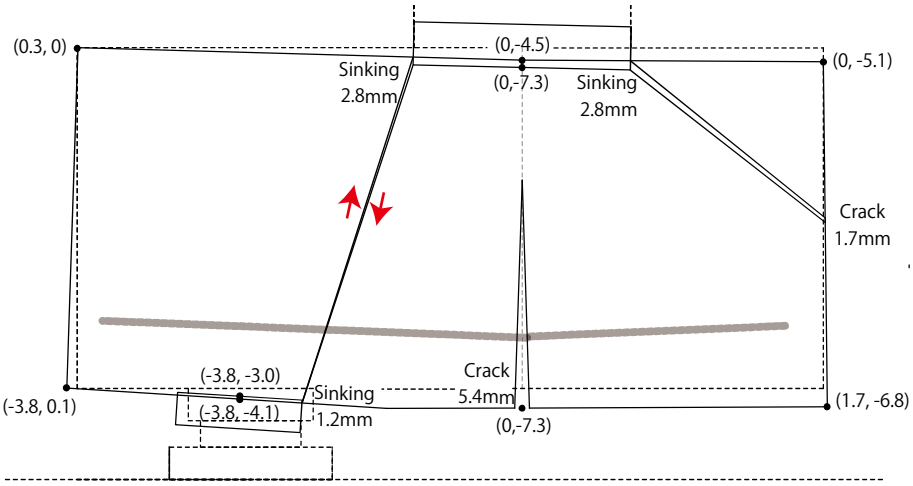

(a) Assuming sliding

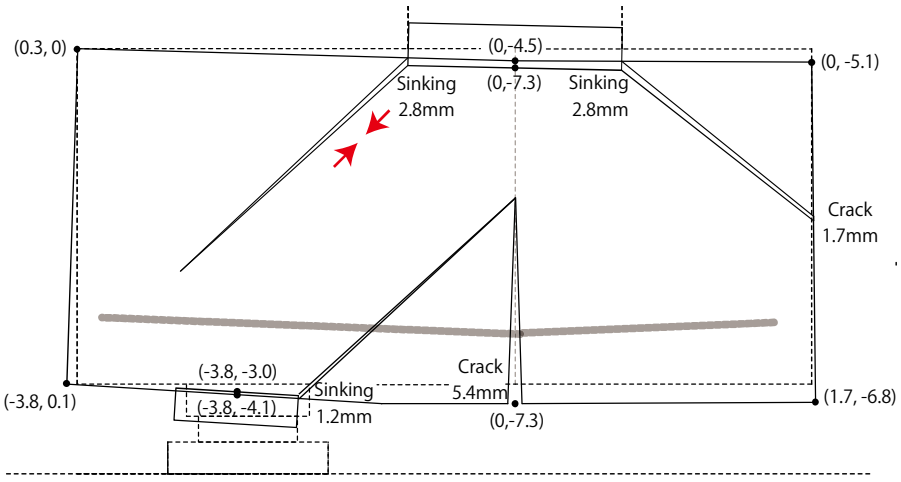

(b) Assuming inclined compressive strain

Fig. 15 – Deformation of specimen L1 at the peak load

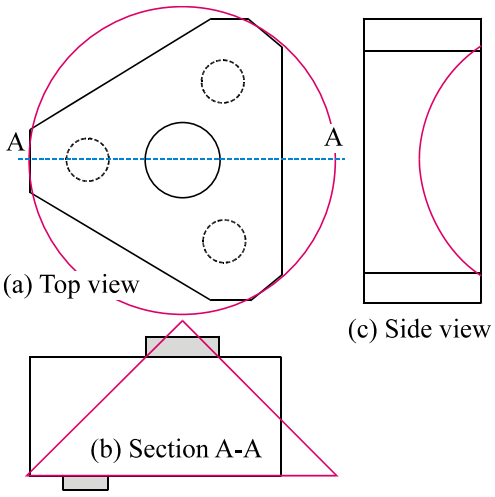

Fig. 16 – Specimen with an imaginary cone

5. Assumed Strain Distribution

Based on the assumptions shown in Fig. 15b, the strain distribution is assumed to be as depicted in Fig. 17. The regions shaded in gray are assumed to be rigid because they are under tri-axial compression. The regions shaded in pink are assumed to have tensile strain. The regions shaded in blue are assumed to have compressive strain. The lengths of these regions, a_{top}, are approximated as follows:

$$a_{top} = \sqrt{2}\left(a + r_{bot} - r_{top}\right) \tag{3}$$

where a is shear span length and r_{bot} and r_{top} are the radii of the bottom and top plates, respectively. Using the strain at the top of the compressive region, ε_{top}, the deformation, e_{top} in Fig. 18, is computed as:

$$e_{top} = \varepsilon_{top} a_{top} \tag{4}$$

The deformation, e_{top} in Fig. 18 can be computed by multiplying the rotation of the compressive region, θ, and the depth of the compressive region, c:

$$e_{top} = \theta c \tag{5}$$

Equations 4 and 5 lead to:

$$\theta = \frac{\varepsilon_{top} a_{top}}{c} \tag{6}$$

Fig. 19 shows the deformation of the bottom face of the specimen. The solid red circle is assumed to expand to the dashed red circle. The expansion, e_{steel}, is given by:

$$e_{steel} = \theta \times (1-k)d \tag{7}$$

where θ is the rotation of the compressive region and $(1-k)d$ is the distance between the origin of the rotation and the reinforcement (Fig. 14). The strain in the red circle in Fig. 19, which is equal to the strain of the reinforcement, is:

$$\varepsilon_{steel} = \frac{e_{steel}}{a} = \frac{\theta \times (1-k)d}{a} \tag{8}$$

The tensile force of the reinforcement is:

$$T = A_{steel} E_{steel} \varepsilon_{steel} \tag{9}$$

where A_{steel} and E_{steel} are the cross-sectional area and Young's modulus of the reinforcement, respectively. Fig. 20 shows distributions of compressive stresses corresponding to strains of 0.001 and 0.003, where E_c is Young's modulus of the concrete and:

$$k_1 = 0.85 - \frac{0.05(f_c - 28)}{7} \geq 0.65 \tag{10}$$

$$k_3 = 0.85 \tag{11}$$

Fig. 21 shows the top plate divided into thirds, each of which supports a compressive strut. Because π is nearly equal to 3, the area of each part is nearly equal to r_{top}^2 as shown by the broken square in Fig. 21. Thus, it is assumed that the width of the compressive strut is equal to the radius of the top plate:

$$b_e = r_{top} \tag{12}$$

The compressive force of the strut is:

$$\text{If } \varepsilon_{top} = 0.001 \text{ then } C = E_c \times 0.001 \times b_e c / 2 \tag{13}$$

$$\text{If } \varepsilon_{top} = 0.003 \text{ then } C = k_1 k_3 f_c b_e c \tag{14}$$

Fig. 22 gives the relationship between the strut depth c and the angle of the rigid zone β:

$$\frac{c}{\cos(\beta - 45)} = \frac{r_{top}}{\cos\beta} \quad \text{or} \quad \frac{\sqrt{2}c}{\cos\beta + \sin\beta} = \frac{r_{top}}{\cos\beta} \quad \text{or} \quad \tan\beta = \frac{\sqrt{2}c}{r_{top}} - 1 \tag{15}$$

Fig. 22 also gives the relationship between the angle of the rigid zone β and the neutral axis depth kd:

$$kd = r_{top} \tan\beta \tag{16}$$

The equilibrium shown in Fig. 1 is still valid and leads to the relationship between C and T:

$$C = 2\sqrt{2} T \cos 30 \tag{17}$$

The vertical force corresponding to the strains of ε_{top} = 0.001 or 0.003 is obtained as follows:

1. Assume depth of compression region, c, such as 0.1d, 0.2d, 0.3d, or 0.4d.
2. Compute tanβ using Eq. 15.
3. Compute kd using Eq. 16.
4. Compute T using Eq. 9.
5. Compute C using Eq. 13 or 14.
6. Check equilibrium using Eq. 17. If equilibrium is satisfied, compute θ and P using Eqs. 6 and 1. If not, go back to step 1.

Fig. 23 shows the computed compressive and tensile regions for ε_{top} = 0.001 or 0.003 and for specimens L3b and L1. The triangles and rectangles shown in broken blue lines represent stress distributions. Note that the compressive zone of specimen L3b is wider than that of specimen L1, although their concrete strengths are similar. This difference is caused by the difference in amount of reinforcement. Fig. 24 compares the observed load-deflection curves with the computed curves. The computed strength of specimen L3b is larger than that of specimen L1, which corresponds to the different width of the compressive zone shown in Fig. 23. We may

conclude that the failure of the specimens was similar to that of over-reinforced beams under flexure. The broken lines in Fig. 24 show the computed load-deformation relationships. They agree with the observed ones shown by the solid curves. This conclusion is reminiscent of the work of Tureyen and Frosch [3], which stated that the shear strength of RC beam is proportional to the depth of neutral axis.

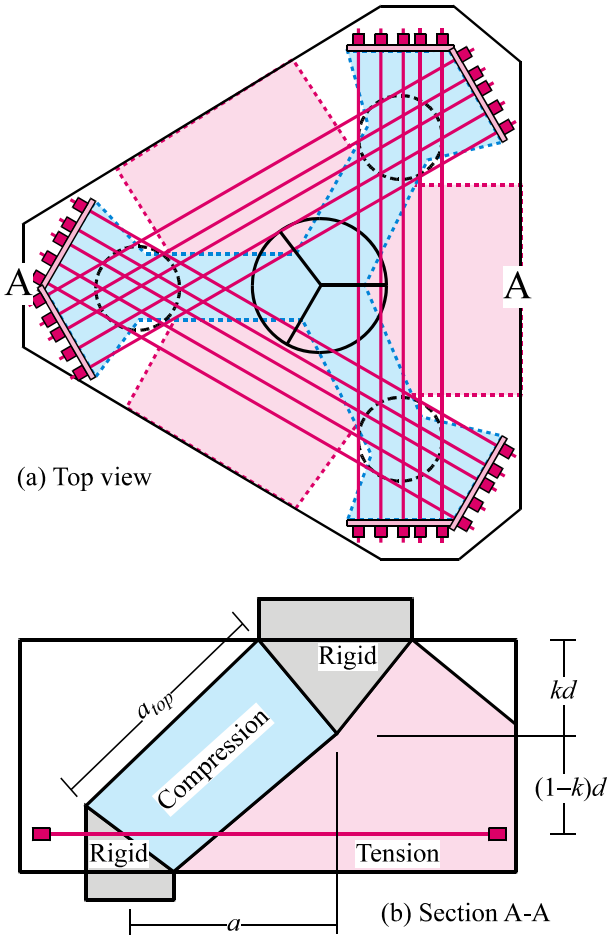

Fig. 17 – Assumed strain distribution.

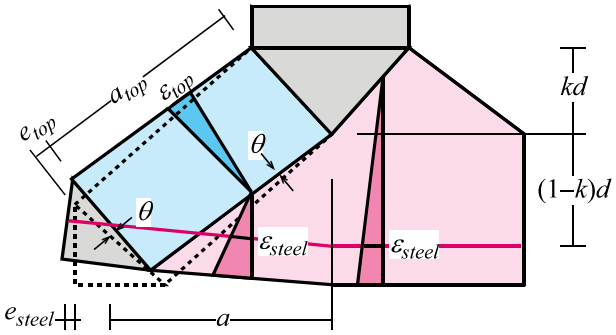

Fig. 18 – Assumed deformation.

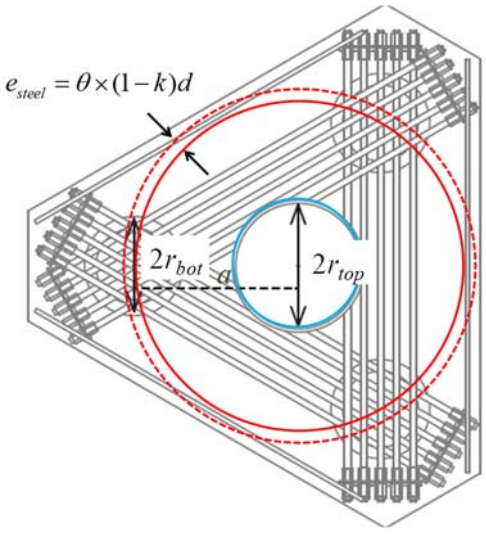

Fig. 19 – Strain of bottom reinforcement

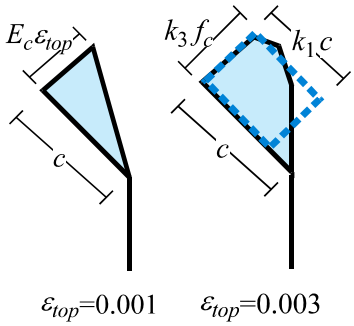

Fig. 20 – Compressive stress of concrete.

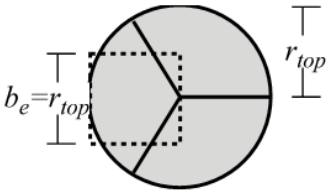

Fig. 21 – Effective width of strut.

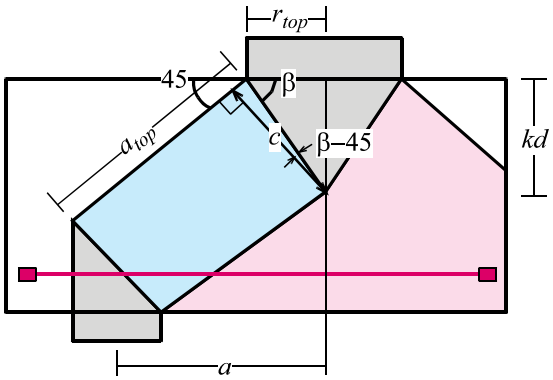

Fig. 22 – Relationship between strut depth *c* and neutral axis depth *kd*.

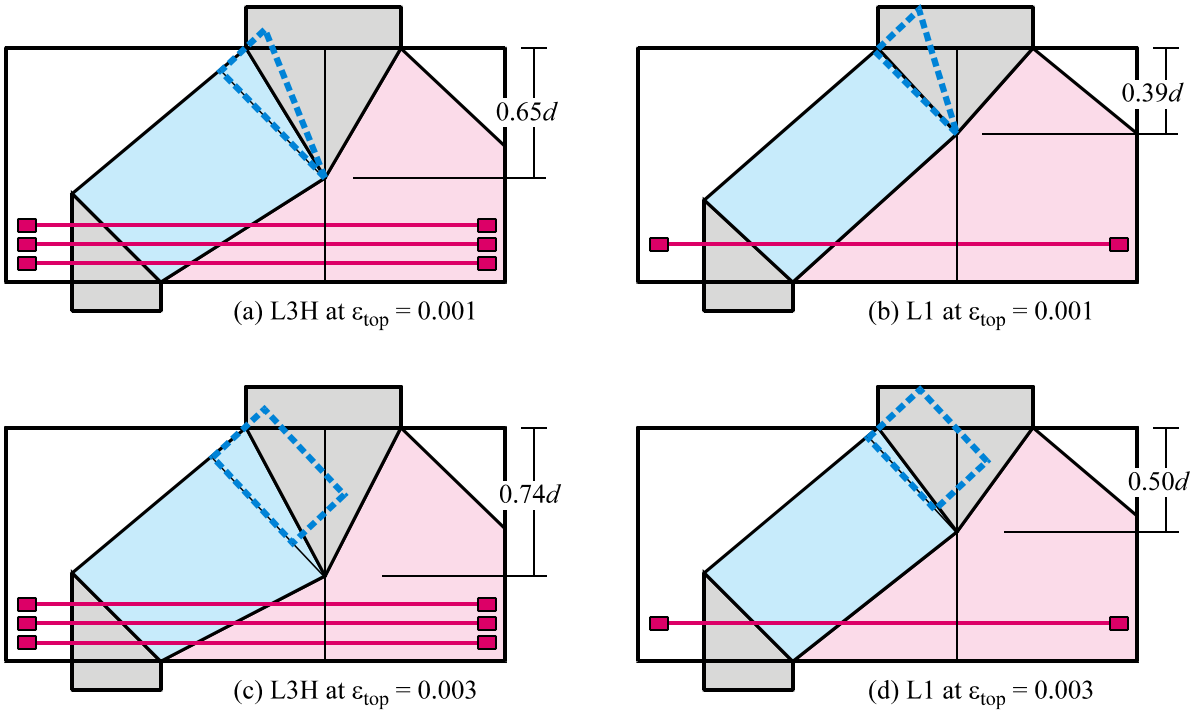

Fig. 23 – Computed neutral axes.

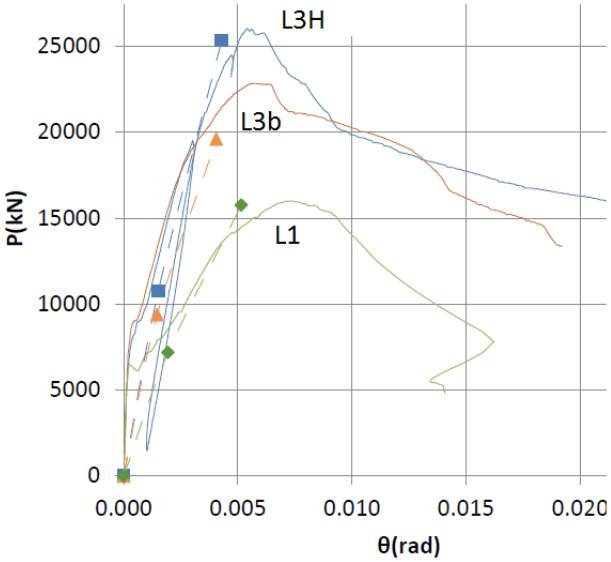

Fig. 24 – Observed and computed load-deformation relationships

6. Conclusions

(1) In all specimens, the bottom reinforcement did not yield. Observed strains in the bottom reinforcement agreed with the predictions of the strut-and-tie model regardless of reinforcement ratio.

(2) Strengths of specimens with three layers of reinforcement were 1.4 times that of the strengths of specimens with one layer of reinforcement. Noting that $3^{1/3} = 1.4$, we may conclude that the strength of pile cap is proportional to the reinforcement ratio to the power of 1/3 as assumed in the equation for the shear strength of RC beam of ACI code [1]. However, this result is not consistent with the conclusion of the strut-and-tie model, assuming that the strength of each strut is independent of the strain of the reinforcement.

(3) If one assumes the specimens deform as shown in Fig. 18, one can obtain estimates of strength similar to the observed values as shown in Fig. 24. This is because the depths of the struts increase as the amount of the bottom reinforcement increases as shown in Fig. 23.

7. References

[1] ACI 318 (2019), "*Building Code Requirements for Structural Concrete*", American Concrete Institute, Farmington Hills.

[2] Nakagami Y, et al (2020): Size effect of footing under two-way shear, Part 3 Deformation, AIJ Tokai Branch, pp. 161-168.

[3] Tureyen, A.K. and Frosch, R.J. (2003): Concrete Shear Strength: Another Perspective, *ACI Structural Journal*, Vol. 100, No. 5, pp. 609-615

8. Acknowledgments

This research was conducted using the fund of Advanced Loading and Real-scale Experimental Mechanics Laboratory (ALREM) supported by KYB, SWCC Showa Cable Systems Co., Ltd., Japan Iron and Steel Federation, Bridgestone, and OILES Corporation. ALREM belongs to Tokyo Institute of Technology, and is directed by Prof. Kazuhiko Kasai. Invaluable advice was given by the members of the ALREM research committee headed by Prof. Akira Wada. The reinforcing bars and anchor devices were provided by Kyoei-Seiko Corporation. Professor Shyh-Jiann Hwang of NCREE, Taiwan, greatly contributed to this project. Dr. Srinivas Mogili of NCREE, Taiwan, supervised cutting of the specimens.

